International Journal of Minerals, Metallurgy and Materials
Volume 19, Number 10, Oct 2012, Page 939
DOI: 10.1007/s12613-012-0651-x

Anodic dissolution of a crack tip at AA2024-T351 in 3.5wt% NaCl solution

Hai Sheng, Chao-fang Dong, Kui Xiao, Xiao-gang Li, and Lin Lu

School of Materials Science and Engineering, University of Science and Technology Beijing, Beijing 100083, China
(Received: 31 October 2011; revised: 8 December 2011; accepted: 15 December2011)

Abstract: The anodic dissolution process of a crack tip at 2024-T351 aluminium alloy (AA2024-T351) was determined by means of scanning Kelvin probe (SKP). Wedge-open loading (WOL) specimens were immersed in a 3.5wt% NaCl solution. After various durations of immersion, the Volta potential distributions around the crack were measured by SKP and the surface morphologies were observed by scanning electron microscopy (SEM). It is found that there is a nonuniform distribution of Volta potential around the crack. Before immersion, the Volta potential at crack tip is more negative than that in other regions. However, after immersion, a converse result occurs with the most positive Volta potential measured at the crack tip. SEM observations demonstrate that the noticeable positive shift of Volta potential results from the formation of corrosion products which deposit around the crack tip. Energy-dispersive spectrometry (EDS) analysis shows that the corrosion products are mainly Al oxide and Cu-rich particles. These observations implicate that the applied stress contributes to the preferential anodic dissolution of the crack tip and the redistribution of Cu.

Keywords: aluminium alloys; crack tips; dissolution; brines; stress corrosion cracking

[*This work was financially supported by the Fundamental Research Funds for the Central Universities (No.FRF-BR-10-037B) and the National Natural Science Foundation of China No.51131005]*.]

1. Introduction

As the primary load-bearing material, high-strength aluminium alloys are widely applied to the aerospace industry because of their attractive properties, such as high strength, low density, and good machining properties [1-2]. Much attention has been paid to the corrosion behaviour of high-strength aluminium alloys under the combined effect of corrosion medium and tensile stress, which may result in stress corrosion cracking [3-4] and corrosion fatigue [5]. Constant efforts [6-8] are made to find out the structural, electrochemical, and mechanical mechanisms that govern the failure process at a crack tip and to identify factors that influence the crack initiation and propagation. However, no consensus has been reached for the governing mechanism. Hahm *et al*. [9] found that applied tensile stress could enhance the electrochemical reactivity of AA2024-T3, and this enhancement increased monotonically with the increase of the applied stress. Kermanidis *et al*. [10] estimated the tensile behaviour of corroded 2024-T351 aluminium alloy (AA2024-T351) specimens by finite element analysis. Magnin *et al.* [11] introduced the concept of critical surface defects to explain the effects of anodic dissolution and hydrogen on the different stages of the stress corrosion cracking (SCC) process for 316L stainless steel. Furthermore, Najjar *et al.* [12] extended the concept of critical surface defects to AA7050 alloy and concluded that the main role of anodic dissolution was to produce the critical defects, which could promote a localized plasticity and, more importantly, provide a fast entry for hydrogen getting into the material and cause subsequent embrittlement. Recently, much more attention has been paid to the electrochemical and mechanical behaviour of the localized region at a crack tip. Cooper and Kelly [13] investigated the chemistry and electrochemistry environment at a crack tip using a suite of mini-electrodes. Shoji and his co-workers [14] formulated a theoreti-

Corresponding author: Xiao-gang Li E-mail: lixiaogang99@263.net

cal equation for SCC growth rate of austenitic alloys in high-temperature water based on crack-tip asymptotic fields and crack-tip transient oxidation kinetics. In general, the interaction between tensile stress and corrosion at a crack tip during the SCC process remains an open issue to the scientific community. So far, there is no acceptable mechanism to describe the effect of stress on electrochemical activity at a crack tip or provide a reasonable explanation to corrosion behaviour in this region.

The objective of this research was to study the influence of applied stress on the electrochemical activity of a crack tip and develop a better understanding for the local corrosion behaviour at the crack tip. In this paper, the evolution of the Volta potential distribution around the crack tip was measured by the scanning Kelvin probe (SKP) technique after wedge-open loading (WOL) tests. Scanning electron microscopy (SEM) and energy-dispersive spectrometry (EDS) were used to characterize the surface morphologies and element composition of corrosion products.

2. Experimental

2.1. Specimens and solution

The chemical composition of AA2024-T351 is presented in Table 1. A WOL specimen was machined according to GB 12445.3—90 with the dimension shown in Fig. 1. The working surface of the specimen was wet ground on emery paper down to 1000 grit subsequently, cleaned by ultrasonic wave in deionized water, and degreased in acetone. The WOL specimen was loaded by a bolt to fix the crack opening, resulting in a constant displacement loading situation. Therefore, the stress was along the short transverse direction (S direction), while the crack propagated along the longitudinal direction (L direction). The bolt was sealed by silica gel to inhibit the galvanic and crevice corrosion between the bolt and the sample. Before immersion, the sample was stored in a desiccator for 24 h for curing of silica gel and reduction of creep.

Table 1. Chemical composition of tested AA2024-T351 **wt%**

Cu	Mg	Mn	Si	Fe	Zn	Ti	Cr	Al
3.8-4.9	1.2-1.8	0.3-0.9	≤0.5	≤0.5	≤0.25	≤0.15	≤0.1	Balance

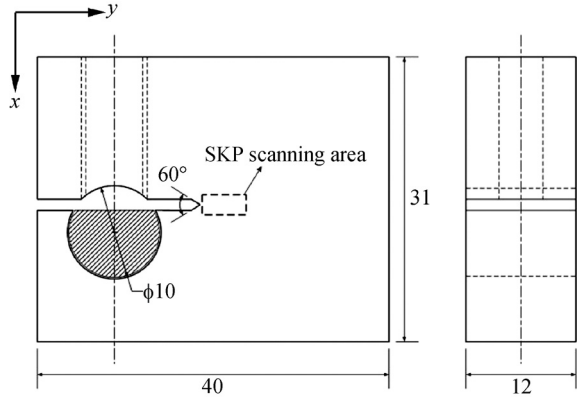

Fig. 1. Schematic diagram of WOL sample (unit: mm).

WOL tests were conducted in a 3.5wt% NaCl solution. The solution was made from analytic-grade reagent and deionized water (0.054 μS/cm). The WOL specimen was immersed in the 3.5wt% NaCl solution for different periods of time. For every 24 h, the solution was changed, and the specimen was cleaned by deionized water and dried for SKP measurements. All the tests were performed at room temperature in the air.

2.2. SKP measurements and SEM observations

After every 24 h immersion, SKP measurement was performed to study the evolution of Volta potential on the working surface of the WOL specimen by M370 scanning electrochemical workstation. In the present study, a tungsten tip of 500 μm in diameter was used to monitor the Volta potential distribution around the crack. The area potential scanning mode was selected. The scanning area was marked by dotted lines in Fig. 1. The step size was 50 and 100 μm along X and Y axes, respectively. The amplitude of probe oscillation was 30 μm and the vibration frequency was set at 80 Hz. The probe tip was calibrated at about 100 μm above the specimen for all measurements.

After SKP measurements, the surface morphologies were investigated by SEM (Quanta FEI 250). Secondary electron images and backscatter electron diffraction (BSED) images were recorded after various immersion periods of time. The element composition for corrosion products was identified by EDS (EDAX A10X).

3. Results

3.1. Volta potential evolution by SKP measurement

Fig. 2 shows the Volta potential distribution on the WOL specimen surface before immersion. The dotted line represents the crack location schematically. It can be seen that

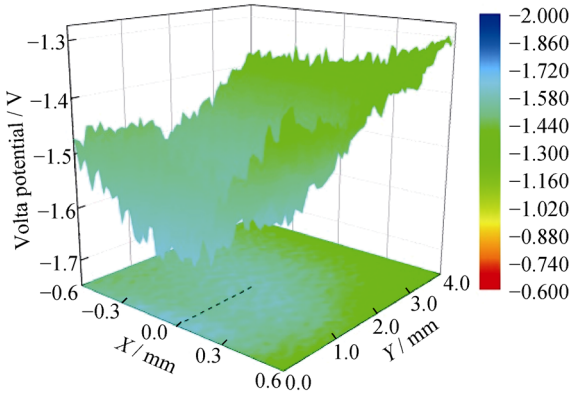

Fig. 2. Volta potential distribution around the crack before immersion with the dotted line representing the crack schematically.

Volta potentials around the crack tip change from −1.58 to −1.72 V, and the Volta potentials of the area away from the crack change from −1.16 to −1.44 V. The average Volta potential of the crack tip is lower than that of the matrix, indicating an anodic character of this area compared to the surrounding matrix.

The contour maps of Volta potential distributions after various immersion periods of time from 24 to 96 h are shown in Fig. 3. For comparison, the contour map of the Volta potential distribution before immersion is presented as well. The dotted lines represent the crack location schematically, with the upper and lower endpoints representing the crack tip and the notch root, respectively. It can be seen that there is an apparent nonuniform distribution of Volta potential after immersion within the SKP scanning area with the most positive values measured nearby the crack tip. With the immersion time increasing, the region with more positive Volta potential expands from the crack tip to the notch root. Comparatively, the Volta potentials away from the crack are found to remain almost unchanged with the increase of immersion time (still within the range from −1.16 to −1.44 V). These results imply that the region nearby the crack is subject to severe corrosion compared to the matrix away from the crack.

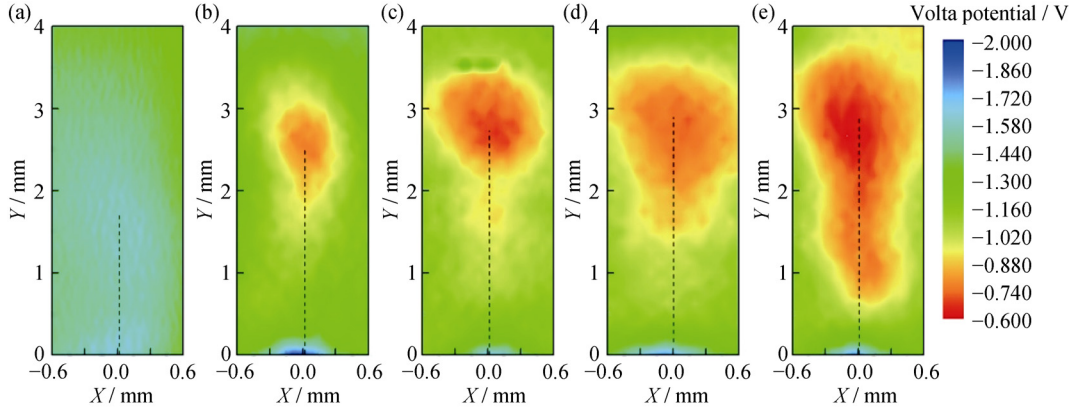

Fig. 3. Volta potential distributions around the crack before immersion (a) and after 24 h (b), 48 h (c), 72 h (d), and 96 h (e) immersion in the 3.5wt% NaCl solution with the dotted lines representing the cracks schematically.

3.2. Surface morphologies and composition analysis

The secondary electron images of the corroded surface after 24 and 96 h immersion in the 3.5wt% NaCl solution are shown in Fig. 4. In Fig. 4(a), it can be found that corrosion products are generated at and ahead the crack tip after 24 h immersion, indicating that the region of the crack tip is subject to corrosion. However, the crack propagates further with the increase of immersion time and the corrosion products can not inhibit this propagation, as shown in Fig. 4(b). Moreover, the region on both sides of the crack is also covered by corrosion products after 96 h immersion.

BSED observations around the crack after 96 h immersion are shown in Fig. 5. Fig. 5(a) shows the BSED image around the crack, in which corrosion products and a great number of fine white particles can be observed. The corrosion products are located on both sides of the crack, while the fine particles are prone to accumulate around the crack tip. Fig. 5(b) reveals the details of surface morphology alongside the crack tip. It is seen that the region nearby the crack is covered by corrosion products, on the top of which the fine white particles are distributed dispersedly. Element composition analysis results by EDS at locations A and B in Fig. 5(b) are listed in Table 2 to estimate the type of corrosion products. The result shows that the corrosion products (location A) are mainly composed of aluminium and oxygen with a small amount of magnesium, indicating that the corrosion products are mainly aluminium oxide. As for the fine white particles (location B), EDS result demonstrates that they are rich in Cu, implying that they are remnants by the

selective dissolution of S phase (Al_2CuMg) [15]. In addition, a small amount of aluminium and oxygen can also be found at location B. This may result from Al oxide beneath the Cu-rich remnant.

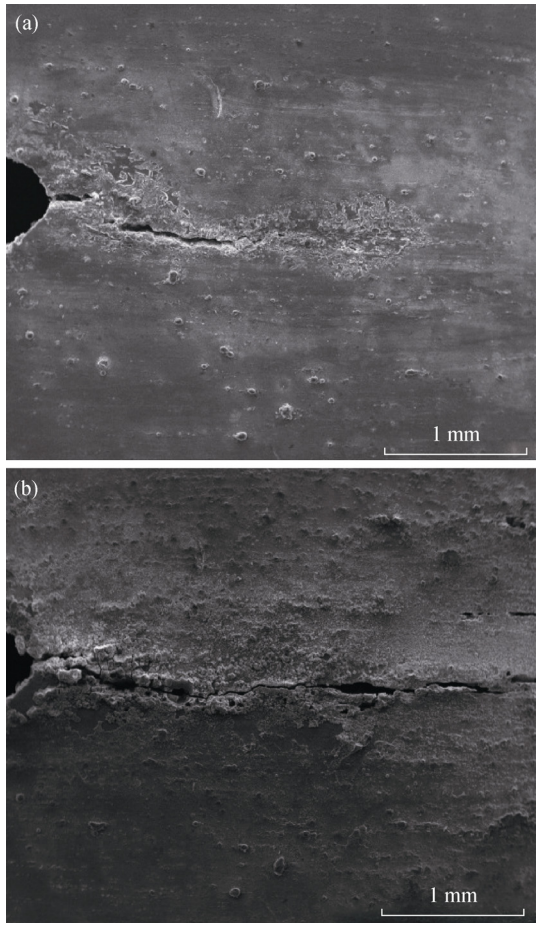

Fig. 4. SEM images of surface morphology after 24 h (a) and 96 h (b) immersion.

4. Discussions

As well known, a singular stress field occurs at the crack tip when the specimen is subject to external tensile stress [16]. This singular stress field is characterized by apparent stress concentration nearby the crack tip, which declines rapidly with the increase of distance from the crack tip. Therefore, the energy of electrons within the region governed by the singular stress field is raised. For SKP measurements, Volta potential represents electron energy on the specimen surface [17]. The local surface region with negative Volta potential indicates its high electron energy, and *vice versa*. As a result, Volta potentials around the crack tip are more negative than that away from the crack before immersion in the 3.5wt% NaCl, as shown in Fig. 2. Under the effect of applied stress, the electron energy of the crack tip is raised high enough for electrons to escape from the metal when the specimen is immersed in the solution. Therefore, the electrochemical activity at the crack tip is enhanced within the singular stress field. Consequently, the region at the crack tip can be seen as an anode with respect to the surrounding matrix. After immersion in the solution, anodic dissolution occurs at the crack tip preferentially and generates corrosion products therein, as shown in Fig. 4(a). In this case, the corrosion products of aluminium alloys in a neutral NaCl solution is mainly composed of Al oxide, and the corresponding reactions are as the following equations [18].

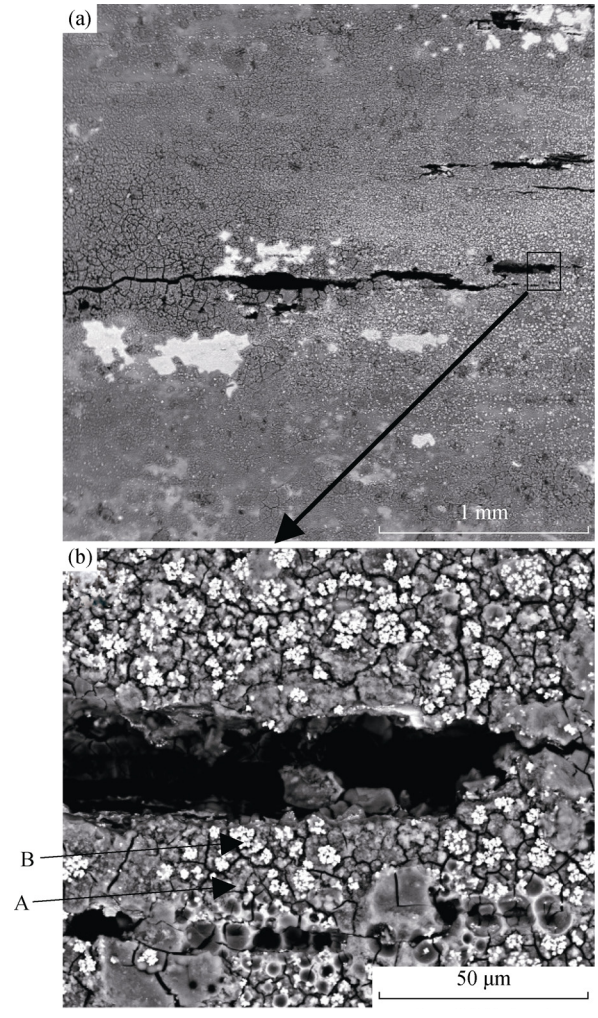

Fig. 5. BSED images after 96 h immersion at lower magnification (a) and higher magnification (b).

Table 2. EDS results of locations A and B in Fig. 5(b) wt%

Location	O	Al	Mg	Cu
A	36.09	62.47	1.44	—
B	5.78	10.23	—	83.98

$$O_2+2H_2O+4e^- \rightarrow 4OH^- \quad (1)$$

$$Al \rightarrow Al^{3+}+3e^- \quad (2)$$

$$Al^{3+}+3OH^- \rightarrow Al(OH)_3 \quad (3)$$

$$2Al+6OH^- \rightarrow Al_2O_3+3H_2O+6e^- \quad (4)$$

The contour maps of Volta potential distributions measured after immersion demonstrate a positive shift of Volta potential of the crack tip, as shown in Fig. 3. Al oxide can be attributed to this positive shift because it has a more positive potential than that of the matrix.

With the immersion time increasing and the crack propagating, the stress intensity factor (K) decreases for the WOL specimen. Therefore, stress concentration and its effect on the enhancement of electrochemical activity at the crack tip decline. As a result, severe corrosion takes place and corrosion products are generated on both sides of the crack, as shown in Fig. 4(b). Consequently, the Volta potentials gradually become more positive from the crack tip to the notch root with the increase of immersion time, as shown in Fig. 3. On the other hand, chloride ions are prone to migrate from the bulk solution into the crack [13]. A chloride-rich and acid environment may develop within the crack and promote corrosion on both sides of the crack, which can also play a vital role in the corrosion process nearby the crack.

Besides the corrosion product of Al oxide, Cu-rich particles are also found around the crack tip. These Cu-rich remnants can be caused by the selective dissolution of Al and Mg from the S phase (Al_2CuMg) particles [15, 19], resulting in the de-alloying of S phase and the enrichment of the surface with Cu, as shown in Fig. 5(a). As the work function under the vacuum condition of Cu (4.70 eV) is higher than that of Al (4.19 eV) [20], the enrichment of Cu around the crack tip can lead to a positive shift of the measured Volta potential. Furthermore, the Cu-rich remnants can act as cathodes compared to the surrounding matrix, as the Cu-rich remnants are nobler than the Al matrix. These noble Cu-rich remnants can also promote the corrosion of the surrounding matrix and generate corrosion products. Therefore, the increase in Volta potential can be partially contributed to these Cu-rich remnants.

Fig. 5(a) shows the heterogeneous distribution of Cu remnants on the surface. Cu particles are prone to accumulate around the crack tip, while a little Cu can be found on both sides of the crack. Buchheit *et al.* [21] reported that some Cu-rich remnants detached from the alloy surface and could be moved by the mechanical action of the growth of hydrous corrosion products or by the solution, which indicated a non-Faradaic liberation of Cu. Observations in Fig. 5(a) suggest that the stresses around the crack tip can induce the non-Faradaic liberation of Cu under the free corrosion condition. Under the effect of stresses, the fine particles rich in Cu are redistributed around the crack tip. However, the mechanism needs to be verified in the further work.

5. Conclusions

(1) The anodic dissolution of a crack tip at AA2024-T351 is enhanced by applied stress. The dissolution process is accompanied by the formation of corrosion products, *i.e.*, Al oxide and Cu-rich remnant, around the crack tip.

(2) A nonuniform distribution of Volta potential is developed around the crack. Before immersion in the 3.5wt% NaCl solution, the most negative Volta potentials are measured at the crack tip. The electrochemical activity and susceptibility to dissolution are enhanced within the region of stress concentration.

(3) After immersion, Volta potentials at the crack tip increase remarkably, which are more positive than those in other regions. This noticeable positive shift of Volta potential can also be contributed to Al oxide and Cu-rich remnants around the crack tip.

References

[1] E.A. Starke Jr. and J.T. Staley, Application of modern aluminum alloys to aircraft, *Prog. Aerosp. Sci.*, 32(1996), No.2-3, p.131.

[2] C.F. Dong, H. Sheng, Y.H. An, X.G. Li, and K. Xiao, Local electrochemical behavior of 2A12 aluminium alloy in the initial stage of atmospheric corrosion under Cl^- conditions, *J. Univ. Sci. Technol. Beijing*, 31(2009), No.7, p.878.

[3] B.J. Connolly and J.R. Scully, Corrosion cracking susceptibility in Al-Li-Cu alloys 2090 and 2096 as a function of isothermal aging time, *Scripta Mater.*, 42(2000), No.11, p.1039.

[4] X. Liu, G.S. Frankel, B. Zoofan, and S.I. Rokhlin, *In-situ* observation of intergranular stress corrosion cracking in AA2024-T3 under constant load conditions, *Corros. Sci.*, 49(2007), No.1, p.139.

[5] K. Jones, S.R. Shinde, P.N. Clark, and D.W. Hoeppner, Effect of prior corrosion on short crack behavior in 2024-T3 aluminum alloy, *Corros. Sci.*, 50(2008), No.9, p.2588.

[6] M. Dixit, R.S. Mishra, and K.K. Sankaran, Structure-property correlations in Al 7050 and Al 7055 high-strength aluminum alloys, *Mater. Sci. Eng., A*, 478(2008), No.1-2, p.163.

[7] N. Birbilis, M.K. Cavanaugh, L. Kovarik, and R.G. Buchheit, Nano-scale dissolution phenomena in Al-Cu-Mg alloys,

Electrochem. Commun., 10(2008), No.1, p.32.

[8] R.G. Song, W. Dietzel, B.J. Zhang, W.J. Liu, M.K. Tseng, and A. Atrens, Stress corrosion cracking and hydrogen embrittlement of an Al-Zn-Mg-Cu alloy, *Acta Mater.*, 52(2004), No.16, p.4727.

[9] J. Hahm and S.J. Sibener, Stress-modified electrochemical reactivity of metallic surfaces: Atomic force microscopy imaging studies of nickel and alloyed aluminum, *Appl. Surf. Sci.*, 161(2000), No.3, p.375.

[10] Al.Th. Kermanidis, D.G. Stamatelos, G.N. Labeas, and Sp.G. Pantelakis, Tensile behaviour of corroded and hydrogen embrittled 2024 T351 aluminum alloy specimen, *Theor. Appl. Fract. Mech.*, 45(2006), No.2, p.148.

[11] T. Magnin, A. Chambreuil, and B. Bayle, The corrosion-enhanced plasticity model for stress corrosion cracking in ductile fcc alloys, *Acta Mater.*, 44(1996), No.4, p.1457.

[12] D. Najjar, T. Magnin, and T.J. Warner, Influence of critical surface defects and localized competition between anodic dissolution and hydrogen effects during stress corrosion cracking of a 7050 aluminium alloy, *Mater. Sci. Eng., A*, 238(1997), No.2, p.293.

[13] K.R. Cooper and R.G. Kelly, Crack tip chemistry and electrochemistry of environmental cracks in AA 7050, *Corros. Sci.*, 49(2007), No.6, p.2636.

[14] T. Shoji, Z. Lu, and H. Murakami, Formulating stress corrosion cracking growth rates by combination of crack tip mechanics and crack tip oxidation kinetics, *Corros. Sci.*, 52(2010), No.3, p.769.

[15] L. Lacroix, L. Ressier, C. Blanc, and G. Mankowski, Statistical study of the corrosion behavior of Al_2CuMg intermetallics in AA2024-T351 by SKPFM, *J. Electrochem. Soc.*, 155(2008), No.1, p.C8.

[16] X. Tang and Y.F. Cheng, Micro-electrochemical characterization of the effect of applied stress on local anodic dissolution behavior of pipeline steel under near-neutral pH condition, *Electrochim. Acta*, 54(2009), No.5, p.1499.

[17] P. Bergveld, J. Hendrikse, and W. Olthuis, Theory and application of the material work function for chemical on the field principle, *Meas. Sci. Technol.*, 9(1998), No.11, p.1801.

[18] C.F. Dong, H. Sheng, Y.H. An, X.G. Li, K. Xiao, and Y.F. Cheng, Corrosion of 7A04 aluminum alloy under defected epoxy coating studied by localized electrochemical impedance spectroscopy, *Prog. Org. Coat.*, 67(2010), No.3, p.269.

[19] T. Suter and R.C. Alkire, Microelectrochemical studies of pit initiation at single inclusions in Al 2024-T3, *J. Electrochem. Soc.*, 148(2001), No.1, p.B36.

[20] J.G. Speight, *Lange's Handbook of Chemistry*, 15th ed., McGraw-Hill Book Company, New York, 2005, p.1.132.

[21] R.G. Buchheit, L.P. Montes, M.A. Martinez, J. Michael, and P.F. Hlava, The electrochemical characteristics of bulk-synthesized Al_2CuMg, *J. Electrochem. Soc.*, 146(1999), No.12, p.4424.